Biochimica et Biophysica Acta, 941 (1988) 130–140
Elsevier

BBA 74007

Kinetic measurements of fusion of phosphatidylserine-containing vesicles by electron microscopy and fluorometry

S.W. Hui [a], S. Nir [b], T.P. Stewart [a,*], L.T. Boni [a,**] and S.K. Huang [a]

[a] *Biophysics Department, Roswell Park Memorial Institute, Buffalo, NY (U.S.A.)*
and [b] *Seagram Center for Soil and Water Sciences, Hebrew University of Jerusalem, Rehovot (Israel)*

(Received 8 September 1987)
(Revised manuscript received 4 January 1988)

Key words: Membrane; Fusion; Fluorescence; Calcium ion; Aggregation; Freeze-fracture

Large unilamellar vesicles (REV) containing phosphatidylserine and phosphatidylethanolamine at a ratio of 1:3 were induced to fuse by adding calcium (4 mM). The kinetics of fusion was monitored by fluorometry using terbium or dipicolinic acid-containing vesicles. The morphology and the states of vesicle aggregation and fusion were examined at approx. 2, 30, 60, 150 and 900 s after calcium addition, by rapid quenching and freeze-fracture electron microscopy. The size and the state of aggregation of vesicles are quantitated from 4000 randomly selected vesicles. The aggregation and fusion kinetics as assayed by fluorescence volume mixing is very well simulated and predicted by the mass action model. The model essentially predicts the time course of the distribution of the aggregates and the increase in size of fused particles as measured by electron microscopy, although in some cases the predicted fusion rate exceeds that by morphometric measurement. No morphological features can be defined as fusion intermediates, although bead-like and rim-like materials may be attributed to the remnants of broken diaphragms between fusion partners.

Introduction

Liposomes provide a model for studying the mechanism of fusion between biological membranes. The understanding of the liposome fusion process is crucial to the use of liposomes for drug delivery and other applications.

There have been many reports on the calcium-induced fusion of liposomes containing anionic lipids. When leakage is not excessive the fusion process can be monitored accurately by the content mixing assays employing fluorescent solutions [1]. The kinetics of fusion may be described by the mass action kinetic model [2,3], which yields the distribution of vesicle aggregation-fusion products at various time points during the fusion process. While the average fusion rate can be obtained by using fluorescence assays, only microscopic observation can provide the direct measurement of dimer, trimer, tetramer, etc. formation during the fusion process.

Since the vesicles under study are mostly submicrometer size, and the fusion area is even smaller, the microscopic monitoring of fusion has to be carried out at the electron microscope level. Conventional sample processing for electron mi-

* Present address: Gaymar Industry, Inc., 10 Centre Drive, Orchard Park, NY 14127, U.S.A.
** Present address: The Liposome Company, Inc., 1 Research Way, Princeton Forrestal Center, Princeton, NJ 08540, U.S.A.

Abbreviations: PS, phosphatidylserine; PE, phosphatidylethanolamine; Tes, 2-{[2-hydroxy-1,1-bis(hydroxymethyl)ethyl]amino}ethanesulfonic acid; DPA, dipicolinic acid.

Correspondence: S.W. Hui, Biophysics Department, Roswell Park Memorial Institute, Buffalo, NY 14263, U.S.A.

croscopy, which requires minutes to hours of fixation and dehydration, is not suitable for this study. With the advance of the rapid-freezing technique [4,5], it is possible to arrest kinetic events at given time points, to the accuracy of milliseconds. This technique has been applied to study the morphology of calcium-induced vesicle fusion at early time points [6–9]. Here we report our quantitative study of mass action kinetics of aggregation and fusion by electron microscopy, and compare the microscopic observation with macroscopic fluorescence measurements, in order to elucidate more details of the membrane fusion process.

Materials and Methods

Vesicle preparation. Phosphatidylserine (PS) from bovine brain, and phosphatidylethanolamine (PE) obtained by transesterification of egg phosphatidylcholine were purchased from Avanti Polar Lipids (Birmingham, AL). Terbium chloride ($TbCl_3$) and dipicolinic acid (DPA) were purchased from Sigma.

Mixed lipid vesicles composed of PS/PE (1 : 3) were made by the reversed-phase evaporation method [10]. For content mixing experiments, vesicles were prepared in either 2.5 mM $TbCl_3$ or in 50 mM DPA, as described previously [11]. All samples were filtered through a 0.2 μm polycarbonate filter. Unencapsulated materials were separated on a Sephadex G-75 column. The final sample concentrations were adjusted to either 150 μM or 313 μM lipid phosphate, for the convenience of parallel fluorometric and electron microscopic experiments. The vesicles were suspended in 100 mM NaCl, 2 mM histidine, 2 mM Tes and 0.1 mM EDTA (pH 7.4).

Fluorometric measurement of fusion and leakage. Mixed Tb- or DPA-containing samples at a ratio of either 1 : 1 or 1 : 10 were placed in a cuvette. 0.5 ml of 20 mM $CaCl_2$ stock solution was injected into the cuvette and rapidly mixed with the vesicle suspension, to a resulting Ca^{2+} concentration of 4 mM. The fluorescence (540 nm) was measured with an Aminco fluorometer, using an excitation at 475 nm. The method is essentially the same as that previously described [11]. The 100% Tb-fluorescence calibration was obtained by lysing all vesicles in 0.5% deoxycholate.

Leakage of vesicle content was measured by following the decrease in fluorescence intensity of pre-encapsulated Tb-DPA complex. The quantity D measures the percent of reduction in the fluorescence intensity following induction of fusion. The quantity F is the measured fluorescence intensity increase relative to maximal. The quantity I denotes the corrected increase in fluorescence intensity relative to maximal, and a 1 : 1 ratio of Tb to DPA vesicles is given by $I = F + \beta D$, where $0.5 < \beta < 1$. Initially, when fused doublets are predominant $\beta = 0.5$. Details of the correction at later stages are given in Refs. 3 and 8.

Analysis of fusion kinetics from content mixing data. The analysis followed the mass-action kinetic model [2,3,12,13], which views the overall fusion reaction as a sequence of two gross steps: aggregation and fusion. Dissociation of aggregates was explicitly considered. The calculations were performed by a recently developed program [14] which extends the previous treatment [3] to higher I values, where I is the percent of maximal fluorescence [1]. The rate constants of aggregation, fusion and dissociation employed are $C_{ij}(M^{-1} \cdot s^{-1})$, $f_{ij}(s^{-1})$ and $D_{ij}(s^{-1})$, respectively, where $i = j = 1$ refers to aggregated dimers or fused doublets. The procedure usually involves the determination of C_{11} by simulating the results for dilute vesicle suspension where the rate of aggregation has a more significant effect on the overall aggregation-fusion reaction. Then the rate constant of fusion, f_{11}, is determined by simulating the results obtained with a concentrated vesicle suspension. The rate constant of dissociation, D_{11}, is determined by focusing on later stages of the reaction, i.e., $I > 15\%$.

Electron microscopy. Samples were rapidly frozen by the copper sandwich method as previously described [5]. For the earliest time point, 0.1 μl each of the vesicle suspension and 8 mM $CaCl_2$ were placed on either sides of the open sandwich. The sides were quickly closed and immediately propelled into cold liquid propane. The freezing was less than 2 s from mixing. For longer time intervals, vesicles and a $CaCl_2$ solution were mixed in test tubes. After a pre-selected interval, the mixture was placed in a sandwich and frozen. In some experiments, the fusion process was stopped by the addition of excess EDTA before freezing.

No cryoprotectant was used in any case. The freezing rate was about 5000 C°/s as measured by a miniature thermal couple.

The samples were stored in liquid nitrogen, fractured in a Polaron 7500 unit at −110°C, and replicated with C and C/Pt using Cressington E-beam guns. The replicas were examined in a Siemens 101 microscope at 40 000 × magnification. Because of the rarity of vesicles at this lipid concentration (150 μM), almost all vesicles observed in replicas were photographed for statistical records. The state of aggregation and the apparent diameter, p, of each vesicle on the fracture plane was measured and categorized. The true diameter, d, of vesicles was deduced by the formula (see Appendix)

$$d = 4p/\pi$$

The statistical distribution and the standard deviation of the mean vesicle diameter for each sample, and the percentage of dimers, trimers, etc. (as visualized on the fracture plane) were determined from at least 150 vesicles for each sample. A total of 500 micrographs taken at various time points were used. More than 4000 vesicles were counted in order to obtain a statistically significant distribution. The experiment was repeated three times on different days, each time with a fresh vesicle preparation. The control samples (without Ca^{2+}) were morphologically identical. The results from three experiments were pooled.

Results

Fusion kinetics monitored by content-mixing

A 3:1 mixture of PE/PS was chosen because of the long-term stability of the fusion products. At 15 min after the addition of Ca^{2+} (4 mM), less than 15% of the content had leaked. This is in contrast to pure PS vesicles which leak out most of their contents under similar conditions [1].

The fusion kinetics of the 3:1 PE/PS system has been measured previously [11], employing a single lipid concentration of 50 μM, which was insufficient for a detailed analysis and was impractical for sampling by freeze-fracture electron microscopy. To compromise between the high concentration demanded by electron microscopy sampling and the low concentration for fluorimetry, we chose 150 M of lipid for parallel electron microscopy and fluorimetric measurements.

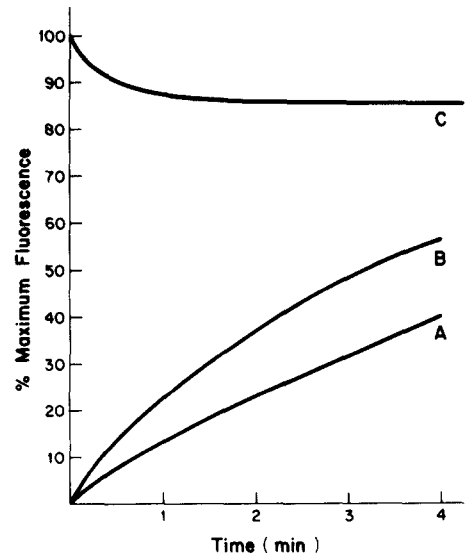

Fig. 1. The fluorescence intensity of mixed PE/PS (3:1) vesicles containing either Tb or dipicolinic acid, at a ratio 1:1 (A) or 1:10 (B) after the addition of 4 mM Ca^{2+}. The curve (C) indicates the loss of fluorescence due to the leakage of encapsulated Tb-dipicolinic acid complex into the EDTA-containing medium.

Fig. 1 shows the changes of fluorimetric intensity, F, after Ca^{2+} was added at time zero to mixed vesicles loaded either with Tb or DPA (at 1:1 and 1:10 ratios for curves A and B, respectively). Curve C is the leakage curve. Both curves A and B show a continuous fluorescence increase due to fusion during 4 min after the Ca^{2+} injection. The net fluorescence intensity, I, curves, after correcting for leakage, are presented in Fig. 2.

If all vesicles in a 1:1 mixture of Tb and DPA vesicles fuse at least once, the corrected fluorescence intensity, I, should reach 50–100% of the maximum intensity, depending on whether the end product consists of predominantly dimers or of high-order fusion products [12]. The I values at infinite time (15 min) indicate that the fusion products may involve more than two vesicles but less than the fusion of the entire population. The most rapid rate of fusion occurs within 30 s of Ca^{2+} injection, although the fluorescence intensity

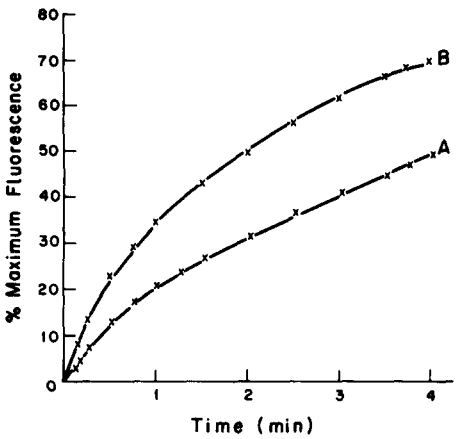

Fig. 2. The net fluorescence intensity, calculated from the measured intensity and leakage shown in Fig. 1. The X points are calculated from the mass-action theory, using the aggregation, fusion and dissociation rate constants given in the text.

at the 30 s time point reaches only 24% and 30% of that at the 4 min time point, for curves A and B, respectively.

A simulation of the fusion kinetics based on the mass action kinetic model was made. The rate constants C_{ij}, f_{ij} and and D_{ij} were determined from the kinetic curves of samples of two different lipid concentrations (150 μM, 313 μM). In the simulation, the calculated I values were obtained by employing the following pre-determined rate constants: $C_{11} = 4 \cdot 10^7$ M^{-1} s^{-1}, $f_{11} = 0.04$ s^{-1}, $D_{11} = 0$. The simulation of I values at the later stages ($I > 15\%$) required setting $f_{ij} = f_{11}/6$ for the higher order-fusion rate constants. An alternative, but less optimal choice of large D_{11} values could not yield a reasonable approximation of the experimental values for the distribution of aggregates, as shown later. The simulation produces exact fittings of the fluorescence data, as shown in Fig. 2.

Electron microscopic studies of aggregation and fusion

The first task for microscopic studies was to demonstrate that the aggregation observed by freeze-fracture electron microscopy was indeed reversible, i.e., dissociatable by the addition of EDTA. The addition of EDTA stopped the fluorescence intensity increase immediately, followed by a slow decrease due to leakage (results not shown), in agreement with previous reports [11,16]. Prior to the addition of calcium, most vesicles were in the monomer state (Fig. 3a). The reversibility of vesicle aggregation was assessed by comparing the morphology of samples frozen-quenched at given time points after calcium injection to the morphology of samples diluted in excess EDTA at the same time points. Fig. 3b and c shows a typical pair of these samples. Most vesicles observed from samples freeze-quenched at 30 s after the Ca^{2+} injection were already aggregated, while those diluted in EDTA at the same time point and then freeze-quenched were predominantly single vesicles (monomers). Apparently, most of the aggregates were dispersed by the addition of excess EDTA. However, the dispersion was not instantaneous. When EDTA was added 10 s after the addition of Ca^{2+}, 13% of the vesicles remained as dimers. The percentage dropped to 5% at 1 min. The calcium-induced aggregation was morphologically distinct from the forced concentration of vesicles by ice-crystal exclusion, which was observed in between the ice crystals and only in highly concentrated and badly ice-damaged samples, independent of sample treatment.

Having established the reversibility of aggregation upon addition of EDTA, we proceeded to quantitate the percentage of vesicles in monomer, dimer, trimer and higher order aggregates at each time point. It should be noted that the sample features are not homogeneous, i.e., several of the same features may be observed at various frequencies at different time points. Fig. 3c–e represent the majority, but not the exclusive features, at these time points. The results are plotted in Fig. 4. Since the theory predicts vesicle numbers and assumes all vesicles are of uniform size initially, the results obtained from polydispersive experimental samples have to be expressed in terms of the percentage of lipids (surface area) rather than the percentage of vesicle counts.

The experimental points in Fig. 4 illustrate the changes of the vesicle distribution due to aggregation and fusion. Initially, before the addition of Ca^{2+}, which induces aggregation and fusion, the distribution consists predominantly of monomers. After 30 s, the number of monomers has significantly dropped due to aggregation, and more than

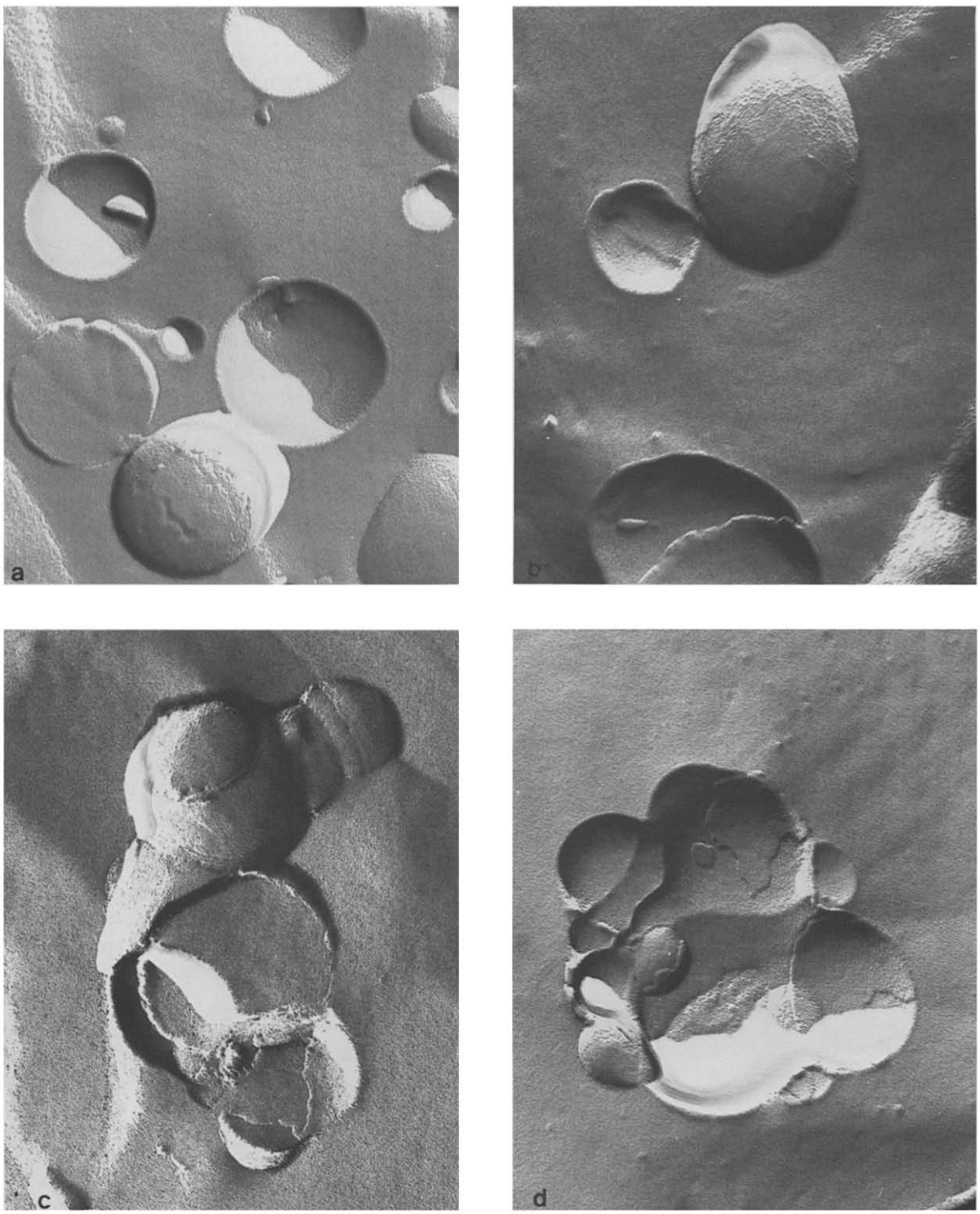

Fig. 3. Typical freeze-fracture electron micrographs of PE/PS (3 : 1) vesicles before (a), and after (b–e) the addition of Ca^{2+}. Excess EDTA was added after 30 s (b), frozen-quenched after 30 s (c), 2 min (d) and 15 min (e) in 4 mM of Ca^{2+}. Bar = 100 nm.

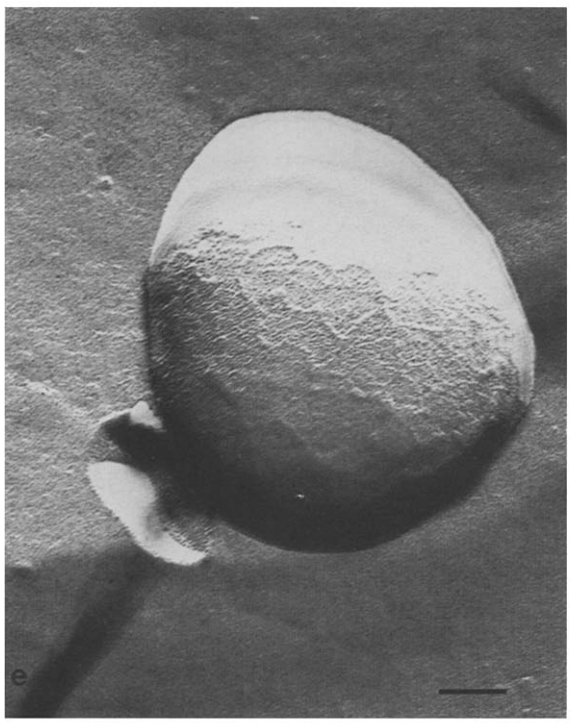

Fig. 3 (continued).

half of the vesicles are found in aggregates of three or more. After 15 min, the monomers again comprise most of the population. The calculations yield the same trend, albeit a significant underestimation of the number of polymers. The explanation of the phenomenon is straightforward. While aggregation reduces the number of monomers, fusion among aggregated vesicles produces

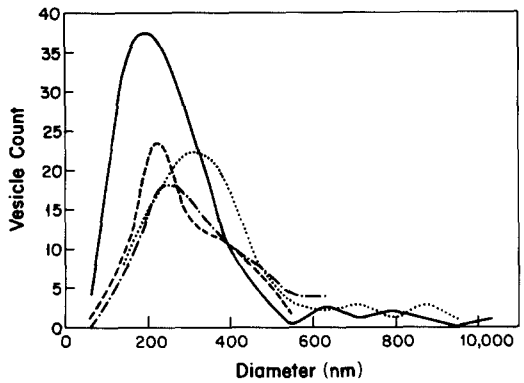

Fig. 5. The size dispersion of vesicles measured by electron microscopy. Vesicle diameters were corrected from cross-section measurements. The curves represent samples of control (pre-calcium) ———, 30 s - - - - - -, 1 min –·–·– and 3 min ····· after the addition of Ca^{2+}.

monomers of larger sizes as the end product. As the overall aggregation-fusion reaction proceeds, more vesicles in an aggregate have a chance to fuse, so that the fraction of monomers rises again at the expense of the high-order aggregates.

The size of vesicles

The cross-fracture size measurement obtained from freeze-fracture electron micrographs represents random cross sections of vesicles at various latitudes rather than the equatorial cross section. The cross-section diameter, p, of the vesicle is related to the equatorial diameter, d, by a stereological correction factor $4/\pi$ (see Appendix).

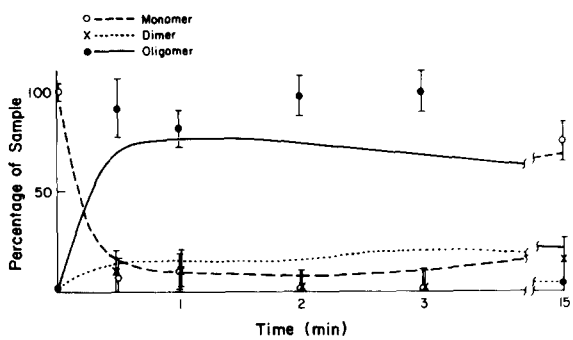

Fig. 4. The changes of the vesicle aggregation state as a function of time, as quantitated from freeze-fracture electron micrographs. The results calculated from the mass-action theory are drawn as smooth curves for comparison.

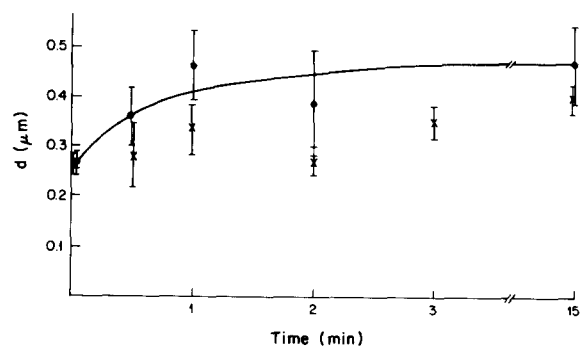

Fig. 6. The mean vesicle diameter at each time point after the addition of Ca^{2+}. The mean values of monomers alone (●) and of all vesicles (×) are drawn separately. The curve is the best fit for monomers.

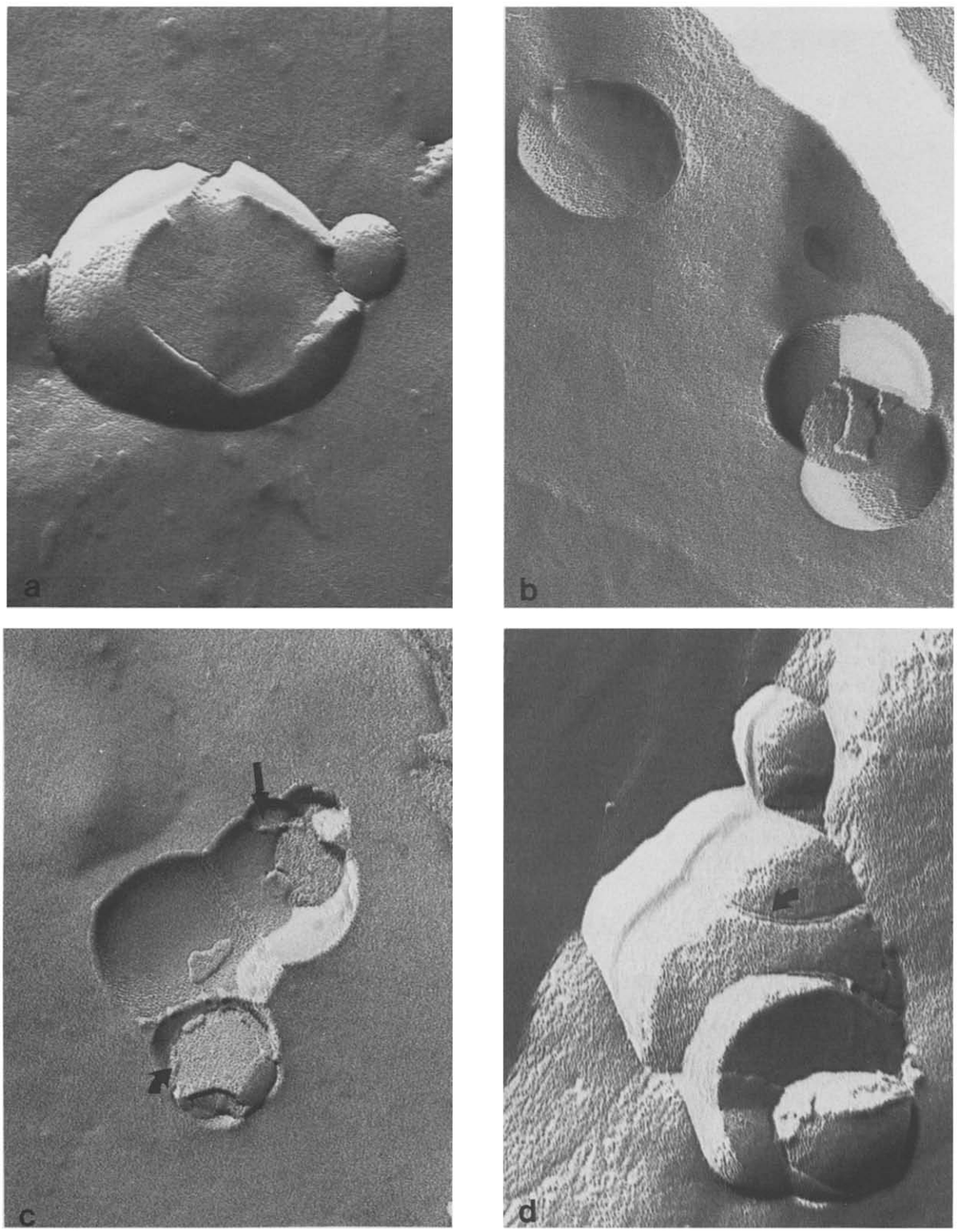

Fig. 7. Detailed structures of fusing PE/PS (3:1) vesicles frozen-quenched at given time points after the addition of calcium (a) 2 s; (b) 37 s; (c) 64 s; (d and e) 154 s. Arrows indicate features possibly representing remnants of fusion, as discussed in the text. Bar = 100 nm.

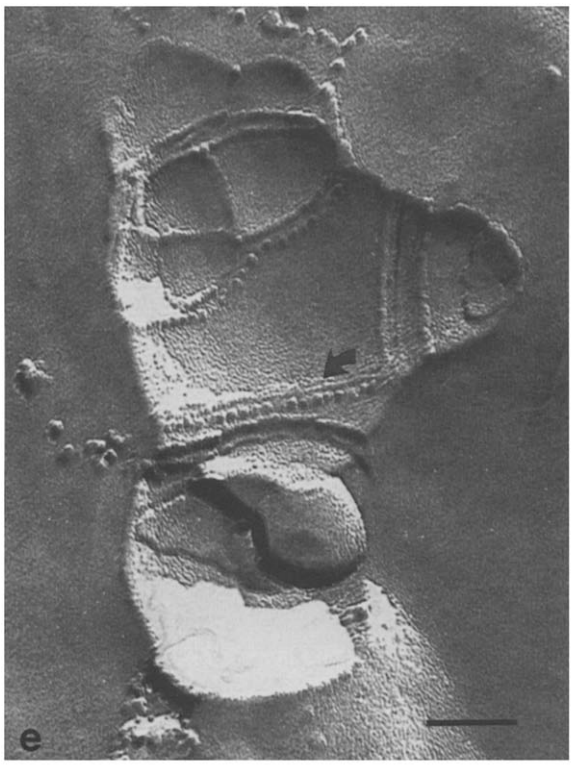

Fig. 7 (continued).

The extremely broad size dispersion, even before the experiment begins, renders mean size measurement inaccurate. This fact is usually overlooked in many reported fusion quantitations, which tend to regard all vesicles as having the same size initially. The degree of polydispersity is illustrated in Fig. 5. The uncertainty due to size dispersion is the main source of error in Figs. 4 and 6).

The size of vesicles increases beyond standard error as a result of fusion. Since monomers are the principal 'end product' at the 15 min time point, their size is categorized separately. The mean sizes of monomers and of all vesicles at each time point are given in Fig. 6.

Within the uncertainty in size, the mean diameter of the monomeric end product is 1.8-times that of the initial monomers. The increase corresponds to a 3-fold surface increase, indicating a 3 : 1 fusion ratio. In other words three vesicles of 200 nm diameter would fuse into one vesicle of 350 nm diameter if the surface was conserved (Fig. 5). However, since monomers are not the only form of the end product, a comparison with the overall mean diameter of all forms of vesicles is more appropriate. The corresponding increase in the mean diameter is 1.5, which translates to roughly a 2.25-fold increase in surface area. The error caused by size polydispersity makes more detailed analysis unwarranted.

Fusion intermediate structures

The fraction of vesicles undergoing fusion at any given time interval, such as the freezing time from t_1 to $t_1 + \Delta t$ is

$$\int_{t_1}^{t_1+\Delta t} (\mathrm{d}f/\mathrm{d}t)\,\mathrm{d}t$$

where $f(t)$ is the fraction of total fusion events that has already occurred at time t. This is true if the life-time of the transient fusion intermediate is shorter than the freezing time Δt. The function $f(t)$ is usually measurable, as given in Fig. 2. The probability to arrest and observe a fusion intermediate by freeze-fracture electron microscopy is then $S[f(t_1 + \Delta t) - f(t_1)]$ where S is the spatial probability that the fracture plane cuts through a fusion site. Since our fusion kinetics, $f(t)$ is rather slow compared to Δt (about 1 ms), the probability is extremely low. The more common structural features shown below may not represent fusion intermediates.

Immediately after the mixing of calcium with vesicles, membrane/membrane contact is observed (Fig. 7a). At 37 s, the contact areas (diaphragms) were widened and flattened, but still consisted of two layers of membranes, as shown in Fig. 7b. The vesicle at the upper left corner probably represents the external view of vesicles in contact. When the contact diaphragm was removed by fusion, there was a remnant of the partitioning membrane in the form of an irregular string of beads on the vesicle wall. At 64 s, some of these partition remnants (beaded strings) were seen to end on the inside wall of the attached vesicles along the contact diaphragm (Fig. 7c). At 2 min 34 s, two forms of feature were seen along the vesicle contact region, a continuous rim (Fig. 7d) or a regular string of beads (Fig. 7e) circumventing a periphery where the partition had

existed. Emphasis is laid again on the heterogeneity of the samples, i.e., the features shown above are not restricted to these time points. No hexagonal II structures were observed at the fusion sites.

Discussion

Although electron microscopy is often used to study the membrane fusion process, it is very seldom applied in a quantitative sense to monitor the kinetic process. On the other hand, spectrometric and fluorometric measurements need the microscopic basis for interpretation, and an incorrect microscopic assumption can lead to serious misinterpretations. The main obstacles in using electron microscopy data quantitatively are poor timing and sampling, and the difficulty in image quantitation. Both of these problems are solved with the modern image analysis technique.

With the advance of the rapid freezing method, it is expected that electron microscopy will be used more often as a dynamic and quantitative tool in membrane research. Our measurement of aggregation, in terms of mapping the kinetics of oligomer formation is such an example. The fusion measurement is less accurate due to the uncertainty in size measurement which is the only microscopic criterion. Nevertheless, the trend in Fig. 6 follows that predicted by fluorescence content mixing in Fig. 2. The polydispersiveness of vesicle sizes (Fig. 5), which is the major source of error in microscopy, is not a serious obstacle in fluorescence content mixing assays.

The quantitative microscopy results indicate that the calculations based on a mass action model can yield simulation and prediction of volume mixing kinetics due to fusion. Furthermore, the calculated distributions of vesicle aggregation agree in general with freeze-fracture results. Initially, most of the vesicles are monomers. Following the addition of Ca^{2+}, dimers, trimers, tetramers, etc. are formed, but at the same time dimers are fused to form a larger monomer, trimers fuse to dimers and then to monomers, etc. The quantity $K = f_{11}/(C_{11}V_o)$, in which V_o is the molar concentration of vesicles, determines whether the aggregation or fusion per se is the rate-limiting step to the overall aggregation-fusion reaction. In the case where lipid concentration is 150 M, $V_o = 1.8 \cdot 10^{-9}$ M, and using $f_{11} = 0.04\ s^{-1}$, and $C_{11} = 4 \cdot 10^7\ M^{-1} \cdot s^{-1}$, yields $K = 0.6$, which means that the actual fusion step is rate limiting step, in which case fusion follows particle aggregation instantaneously. Thus, in this concentrated (150 μM) lipid suspension the calculated I values are very sensitive to f values, which consequently can be sharply defined by the experimental data. While the value $D_{11} = 0$ was employed, it cannot be ruled out that D_{11} might be of the order of 0.001 s^{-1}. Thus, our results do not imply that the aggretation is irreversible, but rather that aggregate dissociation is a relatively slow process in comparison with vesicle fusion, unless excess EDTA is added. It may be noted that a value $D_{11} = 0.01\ s^{-1}$ would yield a sharp disagreement of the calculated distribution with the freeze-fracture results, overestimating the number of monomers and underestimating the number of vesicles in high-order aggregates at $t = 30$ and 60 s. In fact, a lower fusion rate ($f_{11} = 0.02\ s^{-1}$) gives a better fit of the freeze-fracture quantitation, although it deviates from the fluorescence content mixing data. The experimental data also underestimate the number of oligomers, because some aggregation partners may be lost above or below the fracture plane. As Fig. 4 indicates, the calculations based on fluorometric data still capture the time course of the development of vesicle distribution reasonably well. Perfect agreement cannot be expected, because of statistical uncertainty in vesicle numbers in the sampling by random fracture planes studied, and because of the approximate nature of the equations employed, particularly at later times. A better fit may require fine tuning of the higher-order rate constants, i.e., an increase in the number of parameters, whereas our approach has been to capture the essential features with a minimal number of parameters.

A comparison of the results of fusion of our large unilamellar vesicles of PS/PE 1 : 3 with those previously obtained for the fusion of pure PS vesicles indicates the following characteristics. The overall fusion rate of pure PS vesicles appears to be faster than that of PS/PE 1 : 3 vesicles. However, the rate constants C_{11} and f_{11} are similar and dissociation of aggregates at room temperature is not a major effect in both cases [2,3,13,15–18]. For instance, in the presence of 5

mM Ca^{2+}, C_{11} and f_{11} values reported for PS large unilamellar vesicles are $6.5 \cdot 10^7$ $M^{-1} \cdot s^{-1}$ and 0.08 s^{-1}, respectively. In the presence of 4 mM Ca^{2+}, the corresponding values found are [19] $C_{11} = 3.3 \cdot 10^7$ $M^{-1} \cdot s^{-1}$, $f_{11} = 0.05$ s^{-1}, and $d_{11} = 0$. In contrast, our simulation required the reduction the higher-order fusion rate constants, i.e., $f_{ij} = f_{11}/6$. This means that the Ca^{2+}-induced fusion of PS/PE is initially very similar to that of pure PS, but later on it slows down. In contrast to PS vesicles that exhibit a large degree of leakage initially and collapse at the later stages, PS/PE vesicles retain more than 85% of their contents 5 min following induction of fusion. Initially, the leakage associated with Ca^{2+}-induced fusion of PS/PE 1 : 3 vesicles is about one half of that of PS vesicles, the criterion for comparison being leakage per fusion, or per fluorescence increase [2].

Recent studies on Ca^{2+}-induced fusion of PS vesicles demonstrated a steep increase of f values as a function of Ca^{2+} bound per PS. The expected binding ratio of Ca^{2+}/PS is significantly less in PS/PE 1 : 3 vesicles than in pure PS vesicles [2,15,16]. Hence, the fact that f_{11} values for PS are equal to those for PS/PE can be interpreted to indicate that the addition of PE to PS makes the vesicles more fusogenic in the first round of fusion. It has also been reported in previous studies that addition of PE to certain phospholipid mixtures promotes membrane fusion [11,20,21].

The non-bilayer structures exhibited in PE-containing vesicles have been associated with fusion [22]. We did not observe any hexagonal II phase in any of our freeze-fracture electron micrographs. The bead-like lipidic particles appeared not at the high fusion rate time point of 30 s, but rather at the later time points of 64 and 154 s. This finding is in agreement with others [6–8] who also failed to see any non-bilayer intermediates at the calcium-induced vesicle fusion sites. It is possible that the fusion time is too short, or that the fusion is too unsynchronized to give a significant probability at any given moment. The time, Δt, taken to cool the sample from room temperature to say $-20\,^{\circ}C$ is about 1 ms. The value $[f(t_1 + \Delta t) - f(t_1)]$ is at most, a fraction of 1%. The S probability is likely to be less than 0.1. Therefore, the failure to catch a fusion intermediate by rapid freeze is not surprising.

The 'beads' and 'rims' (on collar) which can be observed in Fig. 7 were also reported by Kachar et al. [9] who proposed a model to explain their observation. These rims and ordered strings of beads (Fig. 7e) could be excess membrane materials accumulated around the broken partition. It is, however, interesting to note that the beads become more continuous as time passes, due, perhaps, to more material being accumulated at a later time point. However, the beads cannot be the fusion intermediate, since more of them are seen later, when fusion slows down.

In conclusion, our quantitative microscopy and fluorescence experiments have shown that the mass-action fusion kinetics is microscopically correct. The morphological data support the aggregation-fusion time sequence deduced from macroscopic measurements.

Acknowledgements

We wish to thank Drs. J. Bentz and N. Duzgunes for helpful discussion, and T. Isac, C.M. Stewart and A. Corsi for technical assistance. This work is supported by grants GM 28120 and GM 30969 from the NIH (S.W.H.) and partially supported by the United States-Israel Binational Science Foundation (BSF), grant 86-00010 and NIH grant GM 31506 (S.N.).

Appendix

Assume a sphere of radius, a, cut by parallel planes. The cross-section discs have radii, y, given by

$$y = \sqrt{a^2 - x^2}$$

where x is the perpendicular distance from the center of the sphere to the discs. The average value of y over the entire height of the sphere from $(-a)$ to $(+a)$ is

$$\bar{y} = \frac{1}{2a} \int_{-a}^{a} \sqrt{a^2 - x^2}\, dx$$

Evaluation of the integral gives

$$\bar{y} = \pi a / 4$$

or in terms of the diameters of the vesicle and of the cross section, d and p, respectively

$$d = 4p/\pi$$

References

1 Wilschut, J., Duzgunes, N., Fraley, R. and Papahadjopoulos, D. (1980) Biochemistry 19, 6011–6021.
2 Nir, S., Bentz, J., Wilschut, J. and Duzgunes, N. (1983) Prog. Surf. Sci. 13, 1–124.
3 Bentz, J., Nir, S. and Wilschut, J. (1983) Colloids Surf. 6, 333–363.
4 Heuser, J.E. and Reese, T.S. (1981) J. Cell Biol. 88, 564–580.
5 Stenger, D.A. and Hui, S.W. (1986) J. Membr. Biol. 94, 43–53.
6 Bearer, E.L., Duzgunes, N., Friend, D.S. and Papahadjopoulos, D. (1983) Biochim. Biophys. Acta 693, 93–98.
7 Miller, D.C. and Dahl, G.P. (1982) Biochim. Biophys. Acta 689, 165–169.
8 Rand, R.P., Kachar, B. and Reese, T.S. (1985) Biophys. J. 47, 483–489.
9 Kachar, B., Fuller, N. and Rand, R.P. (1986) Biophys. J. 50, 779–788.
10 Szoka, F., Olson, F., Heath, T., Vail, W., Mayhew, E. and Papadjopoulos, D. (1980) Biochim. Biophys. Acta 601, 559–564.
11 Duzgunes, N., Wilschut, J., Fraley, R. and Papahadjopoulos, D. (1981) Biochim. Biophys. Acta 642, 182–195.
12 Nir, S., Bentz, J. and Wilschut, J. (1980) Biochemistry 19, 6030–6036.
13 Nir, S., Wilschut, J. and Bentz, J. (1982) Biochim. Biophys. Acta 688, 275–278.
14 Nir, S., Stegmann, T. and Wilschut, J. (1986) Biochemistry 25, 257–266.
15 Nir, S., Duzgunes, N. and Bentz, J. (1983) Biochim. Biophys. Acta 735, 160–172.
16 Bentz, J., Duzgunes, N. and Nir, S. (1983) Biochemistry 22, 3320–3330.
17 Bentz, J., Duzgunes, N. and Nir, S. (1985) Biochemistry 24, 1064–1072.
18 Wilschut, J., Scholma, J., Bental, M., Hoekstra, D. and Nir, S. (1985) Biochim. Biophys. Acta 821, 45–55.
19 Bental, M., Wilschut, J., Scholma, J. and Nir, S. (1987) Biochim. Biophys. Acta 898, 239–247.
20 Gad, A.E., Broza, R. and Eytan, G.D. (1979) Biochim. Biophys. Acta 556, 181–195.
21 Duzgunes, N. (1985) Subcell. Biochemistry 11, 195–286.
22 Hui, S.W., Stewart, T.P., Boni, L.T. and Yeagle (1981) Science 212, 921–923.